Mixing of Particles in Gas–Liquid–Solid Fluidized Beds Containing a Binary Mixture of Particles

ARTICLE *in* INDUSTRIAL & ENGINEERING CHEMISTRY RESEARCH · AUGUST 1998

Impact Factor: 2.59 · DOI: 10.1021/ie9708900

GENERAL RESEARCH

Mixing of Particles in Gas−Liquid−Solid Fluidized Beds Containing a Binary Mixture of Particles

Yong Kang, Myung H. Ko, and Kwang J. Woo

Department of Chemical Engineering, Chungnam National University, Taejon 305-764, Korea

Sang D. Kim

Department of Chemical Engineering, Korea Advanced Institute of Science and Technology, Taejon 305-701, Korea

Soung H. Park, Mutsuo Yashima, and L. T. Fan*

Department of Chemical Engineering, Kansas State University, Manhattan, Kansas 66506-5102

The present study focuses on the axial-mixing characteristics and flow behavior of fluidized particles, which so far have received scant attention compared to the bubbling and flow behavior of fluidizing fluids. On the basis of the axial dispersion model, the mixing coefficients in a gas−liquid−solid fluidized bed with an i.d. of 0.152 m have been estimated from the composition of a binary-particle mixture in the mixing region of the bed. The complex mixing behavior has been interpreted by means of the fractal analysis of pressure fluctuations generated in the bed. It has been found that the axial-mixing coefficient increases with an increase in the gas flow rate or the particle size and that it exhibits a local maximum with respect to the variation of the liquid flow rate. The Hurst exponent recovered from the Pox diagram of pressure fluctuations decreases with increasing gas flow rate, but it displays a local maximum with variation of the liquid flow rate in the bed containing a binary mixture of particles. The axial-mixing coefficient has been correlated in terms of the operating variables. Moreover, a correlation has been obtained, which includes the Peclect number containing the mixing coefficient and the dimensionless groups derived from the isotropic turbulence theory.

Introduction

The increasing applications of gas−liquid−solid fluidized beds in the chemical and allied industries have hastened attempts to explore and analyze the multiphase flow and contacting in these beds. Fluidized solid particles form a dispersed phase in any fluidized bed; these particles often comprise the major fraction of the bed in terms of mass or weight. Hence, it is highly plausible that the bed's hydrodynamic characteristics are strongly dependent on the mixing and flow behavior of the particles. In fact, it has been well recognized that the physical properties, holdup, and distribution of the particles are dominant parameters that need be taken into account in determining the bed expansion and the rates of heat and mass transfer in the bed; in addition, the bubble motion and its characteristics are profoundly influenced by the mixing and flow behavior of particles having the propensity to break up or disperse the bubbles (Fan, 1989; Kim and Kang, 1996). Nevertheless, the particles' mixing and flow behavior so far has received relatively little attention, although knowledge of it is essential for the optimal design and operation of a gas−liquid−solid fluidized bed functioning as a reactor or contactor.

Evstroperva et al. (1972) experimentally measured movements of particles in a gas−liquid−solid fluidized bed. They have obtained the average velocity and mean-square value of the fluctuation component of the tracer-particle motion. The axial mixing and segregation of particles in gas−liquid−solid fluidized beds of binary-particle mixtures were investigated by Fan et al. (1984, 1985, 1987). The pattern of particle mixing has been found to vary according to the flow regimes of bubbles in the beds. Larachi et al. (1995) have reported that the motion of bubble wake and the compensatory descending motion of the emulsion phase consisting of particles and liquid are the major factors affecting particle mixing in the beds.

It has been generally understood that bubbling of the fluidizing gas and turbulence induced by the flow of fluidizing liquid render the particles' mixing and flow behavior exceedingly complex. Notwithstanding the resultant complexity, Kang et al. (1995, 1997) and Luewisuthichat et al. (1995) successfully explored the particles' mixing and flow behavior in the beds by resorting to stochastic approaches (Fan et al., 1990, 1991, 1993; Kwon et al., 1994). Specifically, Luewisuthichat et al. (1995) studied the turbulent motion of

* To whom correspondence should be addressed. Phone: 785-532-5584. Fax: 785-532-7372. E-mail: fan@cheme.ksu.edu.

S0888-5885(97)00890-7 CCC: $15.00
Published on Web 08/27/1998

particles by means of the fractal analysis of particle trajectories obtained from direct visualization. Kang et al. (1995) have analyzed the unsteady-state behavior and fluctuations of the particles' movements by extending the notion of relaxation (Yutani et al., 1982). Moreover, they have estimated the axial dispersion coefficients of particles and elucidated the flow behavior in terms of the correlation dimensions resulting from the chaos analysis of pressure fluctuations in the beds of single-size particles (Kang et al., 1997). Their works are certainly indicative of the capability of stochastic analysis of pressure fluctuations to shed light on phenomena such as the mixing and flow of particles occurring in the beds.

The present study focuses on the mixing and flow behavior of particles in gas−liquid−solid fluidized beds containing binary-particle mixtures. Effects of the velocity of fluidizing gas and liquid are elucidated on the basis of the Hurst exponent recovered from the fractal analysis of pressure fluctuations.

Theoretical Section

The conceptual and mathematical bases are given for defining and measuring the particle-mixing coefficient of a binary-particle mixture and for performing the fractal analysis of pressure fluctuations. This is followed by a description of the methods for determining the convective velocity of particles and for estimating the Hurst exponent of the data.

Particle-Mixing Coefficient. In a gas−liquid−solid fluidized bed containing a binary-particle mixture, the flux of particles of either component in the axial direction, N_{Zj}, can be written as (Juma and Richardson, 1983; Fan et al., 1987)

$$N_{Zj} = -D_{pj}\frac{dC_j}{dZ} + \bar{U}_{pj}C_j, \qquad j = \text{SL,SS} \tag{1}$$

where D_{pj}, C_j, and $\bar{U}_{pj}$ are the axial-mixing coefficient, particle concentration, and convective velocity of either component of the particles, respectively.

The net flux of solid particles is negligible at a steady state. The convective velocity, $\bar{U}_{pj}$, of the particles of either component has been defined as the difference between the interstitial velocity of the fluid and the interstitial velocity required to fluidize the particles of this component alone (Juma and Richardson, 1983; Fan et al., 1987); thus, it can be expressed as

$$\bar{U}_{pj} = \frac{U_f}{\epsilon_G + \epsilon_L} - \frac{U_{foj}}{(\epsilon_G + \epsilon_L)_{0j}}, \qquad j = \text{SL, SS} \tag{2}$$

where U_f and U_{f0j} are the effective volumetric flux of fluid in the bed of a binary-particle mixture and that in the bed of single-size particles, respectively. U_f and U_{f0} can be obtained from the following equations (Kang and Kim, 1988):

$$U_f = \left(\frac{\epsilon_G}{\epsilon_G + \epsilon_L}\right)U_G + \left(\frac{\epsilon_G}{\epsilon_G + \epsilon_L}\right)U_L \tag{3}$$

$$U_{f0j} = \left(\frac{\epsilon_G}{\epsilon_G + \epsilon_L}\right)_{0j} U_G + \left(\frac{\epsilon_G}{\epsilon_G + \epsilon_L}\right)_{0j} U_L, \qquad j = \text{SL, SS} \tag{4}$$

As will be elaborated later, $\bar{U}_{pj}$ can be correlated linearly with the bed height in the test section, Z. Thus, it can be written as (Juma and Richardson, 1983; Fan et al., 1987)

$$\bar{U}_{pj} = a_j + b_j Z, \qquad j = \text{SL, SS} \tag{5}$$

Hence, eqs 1 and 5 lead to

$$D_{pj}\frac{dC_j}{dZ} = (a_j + b_j Z)C_j, \qquad j = \text{SL, SS} \tag{6}$$

Fractal Analysis of Pressure Fluctuations. For a given time series of recorded pressure fluctuations, $X(t)$, spaced in time from $t = 1$ to $t = T$, $X^*(t)$ can be defined as (Feder, 1988; Fan et al., 1990, 1991, 1993; Kwon et al., 1994)

$$X^*(t) = \sum_{u=1}^{t} X(u) \tag{7}$$

Then, the average of recorded signals within the subrecord from time $t + 1$ to time $t + \tau$ is

$$\frac{1}{\tau}[X^*(t+\tau) - X^*(t)] \tag{8}$$

Let $B(t,u)$ denote the cumulative departure of $X(t+u)$ from the average for the subrecord between time $t + 1$ and time $t + \tau$; note that by definition

$$B(t,u) = [X^*(t+u) - X^*(t)] - (u/\tau)[X^*(t+\tau) - X^*(t)] \tag{9}$$

The sample sequential range, $R(t,\tau)$, is defined as

$$R(t,\tau) = \underset{0\le u\le r}{\text{Max}}\, B(t,u) - \underset{0\le u\le r}{\text{Min}}\, B(t,u) \tag{10}$$

By letting $S^2(t,\tau)$ be a sample sequential variance of the subrecord from time $t + 1$ to time $t + \tau$, we have

$$S^2(t,\tau) = \frac{1}{\tau}\sum_{u=t+1}^{t+\tau} X^2(u) - \left[\frac{1}{\tau}\sum_{u=t+1}^{t+\tau} X(u)\right]^2 \tag{11}$$

The ratio $R(t,\tau)/S(t,\tau)$, termed the rescaled range, has been found to scale as a power function of τ, i.e., (Feder, 1988)

$$\frac{R(t,\tau)}{S(t,\tau)} \propto \tau^H \tag{12}$$

If the signal is random and self-affine, the resultant time series exhibits a long-term correlation when $0.5 < H < 1.0$. The value of the Hurst exponent, H, can be evaluated from the log−log plot of R/S against time lag; these plots are known as the "Pox diagram".

Experimental Section

A description is given of materials, facilities, and procedures.

Materials. Air and water were the fluidizing gas and liquid, respectively, and spherical glass beads served as the fluidized particles. The particle diameter was in the range of $(1.0-6.0) \times 10^{-3}$ m, and its density was 2500 kg/m^3. Equal amounts of different size particles by

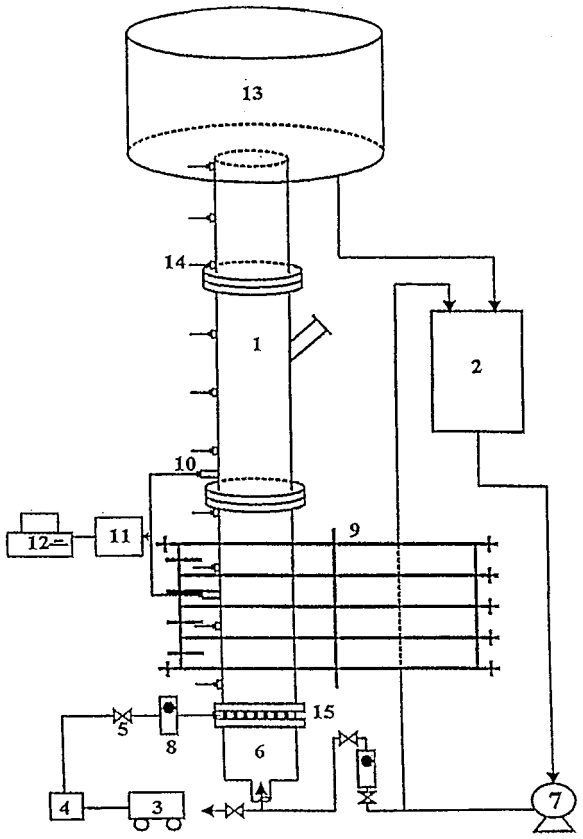

Figure 1. Experimental apparatus: 1, column; 2, reservoir; 3, compressor; 4, filter & regulator; 5, valve; 6, calming section; 7, pump; 8, rotameter; 9, sampling plate; 10, pressure transducer; 11, A/D convertor; 12, PC; 13, weir; 14, pressure taps; 15, distributor.

weight are fed to the column to establish a binary system at each experimental run. The gas and liquid flow rates were in the ranges of 0.01−0.07 and 0.06−0.18 m/s, respectively.

Facilities. Experiments were carried out in an acrylic column of 0.152 m i.d. and 2.5 m height. The length of the test section was 0.6 m, which was divided into five parts (Figure 1). Other details of the experimental apparatus can be found elsewhere (Kang et al., 1995, 1996).

Procedures. The pressure drop in an individual part of the test section was measured by means of the pressure sensor flush mounted on the wall of the column. To measure the local solid holdups, ϵ_{SLi} and ϵ_{SSi}, in the individual part of the test section, five sliding plate samplers were fitted to the side of the column in the test section (Al-Dibouni and Garside, 1979; Juma and Richardson, 1983). The locations of the samplers were 0.15, 0.225, 0.30, 0.45, and 0.60 m from the distributor.

Under given steady-state operating conditions, all the sliders were pushed simultaneously into the bed. Each part of the test section was then dismantled, and the numbers of the larger and smaller particles trapped in it were determined separately. The phase holdups in each part were calculated from the following equations.

$$\epsilon_{Gi} + \epsilon_{Li} + \epsilon_{SLi} + \epsilon_{SSi} = 1.0 \tag{13}$$

$$-\left(\frac{\Delta P}{L}\right)_i = (\epsilon_G\rho_G + \epsilon_L\rho_L + \epsilon_{SL}\rho_{SL} + \epsilon_{SS}\rho_{SS})_i g \tag{14}$$

$$\epsilon_{SLi} = \frac{W_{SLi}}{AL_i\rho_{SL}} \tag{15}$$

$$\epsilon_{SSi} = \frac{W_{SSi}}{AL_i\rho_{SS}} \tag{16}$$

Pressure-fluctuation signals from the pressure sensor were amplified and were recorded by a personal computer from which histograms were constructed. The pressure sensor was of a semiconductor type (Copel Electronics), which was sufficiently fast to follow the dynamic fluctuations of pressure in the beds. The location of the pressure sensor was flush-mounted on the wall of the sampling section, 0.2 m above the gas−liquid distributor. The voltage−time signal, corresponding to the pressure−time signal, from the pressure transducer was fed to the recording system at the selected sampling rate of 0.032 s. A typical sample comprised 3000 points. This combination of sampling rate and time ensured that the full spectrum of hydrodynamic signals was captured from the gas−liquid−solid fluidized beds containing a binary-particle mixture. The signal was processed by a data acquisition system (Data Precision model D-6000) and a personal computer. The signals were processed off-line.

Results and Discussion

The experiments generated the records of pressure drops, phase holdups, concentration profiles, and pressure fluctuations as functions of the operating parameters, including the gas flow rate, the liquid flow rate, and the particle size. The analysis of results has yielded the particle-mixing coefficients of particles of various sizes and the fractal characteristics of pressure fluctuations in terms of the Hurst coefficients. Moreover, two correlations have been obtained for the particle-mixing coefficients: one is empirical in dimensional form, and the other is mechanistic in dimensionless form.

Mixing Zone and Convective Velocity of Particles. The upper bound of the mixing zone in a bed has been determined as the position at which the concentration of smaller particles (floatsam), C_{SS}, is nearly identical with that in the upper bulk region where the smaller particles predominate. The lower bound has been determined similarly as the position at which the concentration of the larger particles (jetsam), C_{SL}, approaches that in the lower bulk region where the larger particles predominate. The relative axial position of the bed varies according to the experimental conditions such as the composition of the particle mixture, the gas flow rate, U_G, and the liquid flow rates, U_L. Thus, Z is defined only in the mixing zone under given experimental conditions.

With the magnitude of each section in the mixing zone, L_i, the measured pressure drop, $(-\Delta P)_i$, and the particle holdups, ϵ_{SSi} and ϵ_{SLi}, known, the holdup of the gas phase, ϵ_{Gi}, and that of the liquid phase, ϵ_{Li} (see Figure 2), have been evaluated by solving eqs 13 and 14 simultaneously. Illustrated in Figure 3 is a typical concentration profile of the particles in the mixing zone along Z.

The bulk or convective velocity of a particle in the axial direction, $\bar{U}_{pj}$, has been evaluated by adapting the method originally developed for liquid−solid beds (Al-Dibouni and Garside, 1979; Juma and Richardson, 1983) and also for gas−liquid−solid beds (Fan et al., 1987;

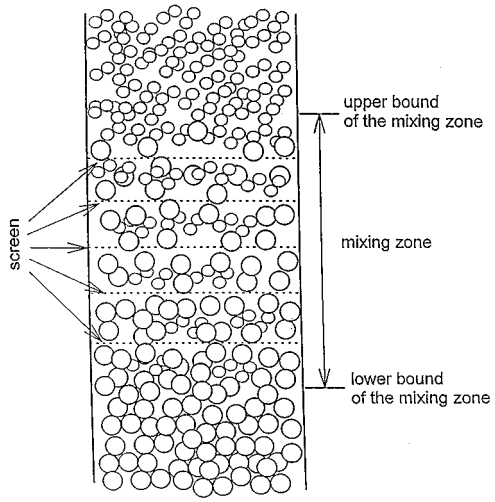

Figure 2. Diagram of the mixing zone.

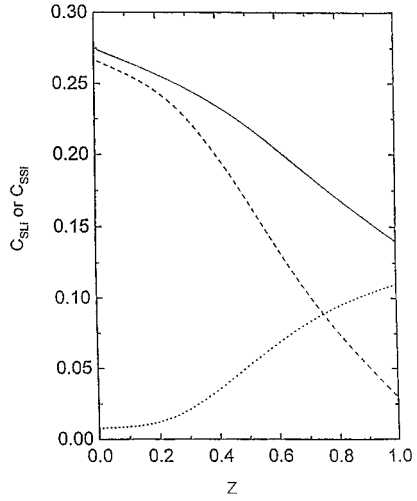

Figure 3. Axial concentration profiles in the mixing zone (U_G = 0.03 m/s, U_L = 0.12 m/s). d_p (mm): (—) 3 + 6, (– –) 6, (···) 3.

Kang and Kim, 1988). The method is based on the relationship between the effective volumetric flux of fluid, U_f, and the bed porosity, $\epsilon_G + \epsilon_L$. The U_f in a gas−liquid−solid fluidized bed of single-size particles or a binary-particle mixture correlates almost linearly with the bed porosity, $\epsilon_G + \epsilon_L$, in log−log plots, as can be seen in Figures 4 and 5, respectively. Thus, similar to eq 4 for the single-size particles, we can write

$$U_{f0j} = K_{0j}(\epsilon_G + \epsilon_L)_{0j}^{n_{0j}}, \qquad j = \text{SL, SS} \qquad (17)$$

for a binary-particle mixture in this expression, where K_{0j} and n_{0j} are constants. With this value of U_{f0j}, $\bar{U}_{pj}$, can be determined from eqs 2−4; the resultant values correlate almost linearly with Z in the mixing zone, as can be seen in Figure 6. A similar dependence of $\bar{U}_{pj}$ on Z has been reported in liquid−solid fluidized beds (Juma and Richardson, 1983) as well as in gas−liquid−solid fluidized beds (Fan et al., 1987).

Axial-Particle-Mixing Coefficient. The axial-mixing coefficient in the mixing zone, D_p, for particles of an individual size has been evaluated from eq 6 by integrating along the height of the mixing zone, Z, with the measured concentration profiles as presented in Figure 3. Figure 7 shows the effects of the gas flow rate, U_G, on D_p of particles of an individual size in the beds

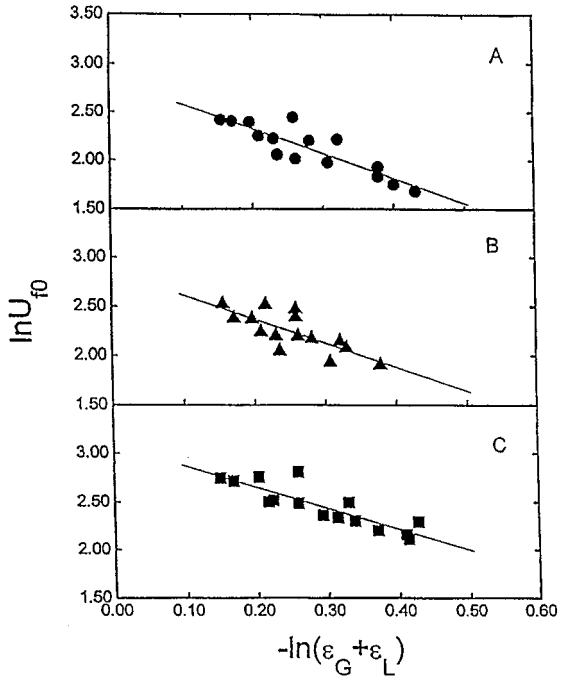

Figure 4. Effective volumetric flux of fluid as a function of the bed porosity in the beds of single-size particles: (A) 1 mm, (B) 3 mm, (C) 6 mm.

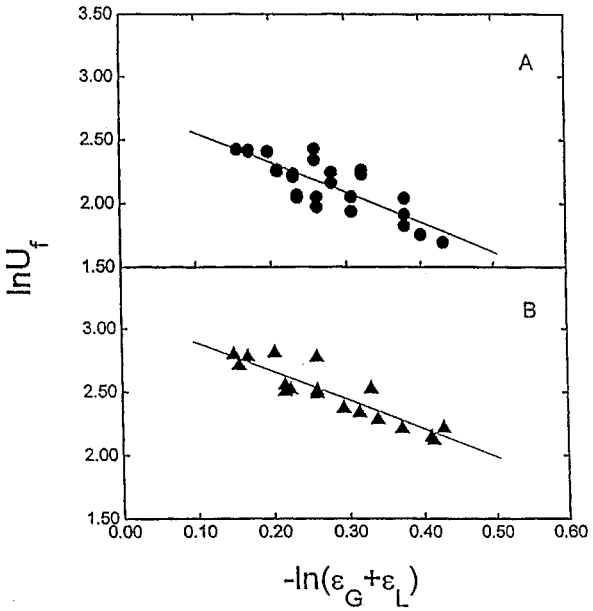

Figure 5. Effective volumetric flux of fluid as a function of the bed porosity in the beds of binary-particle mixtures: (A) 1 + 3 mm, (B) = 3 + 6 mm.

of binary-particle mixtures. Note that D_p increases with an increase in U_G when other operating conditions are fixed. Similar trends have been observed by Fan et al. (1987) in the beds of binary-particle mixtures and Kang et al. (1997) in the beds of single-size particles, both operating in the dispersed-flow regime. This can be due to the enlargement of the bed porosity, $\epsilon_G + \epsilon_L$, thereby inducing the fluidized particles to travel more freely with an increase in U_G. Moreover, the increase in U_G intensifies the turbulence in the bed, which directly affects the mixing and contacting not only among gas, liquid, and particles but also between the particles of different sizes. It is worth noting that the dependency

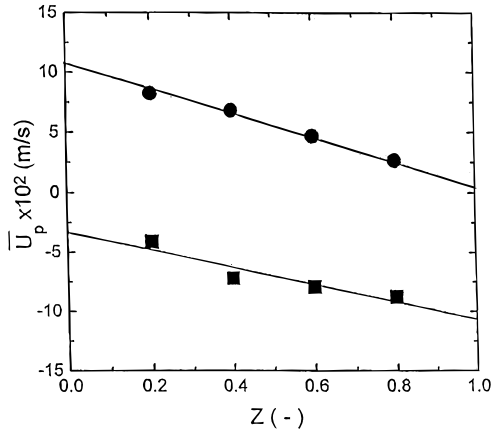

Figure 6. Convective velocity of particles as a function of the dimensionless axial coordinate in the test section (U_G = 0.01 m/s, U_L = 0.10 m/s). d_p (mm): (■) 1; (●) 3.

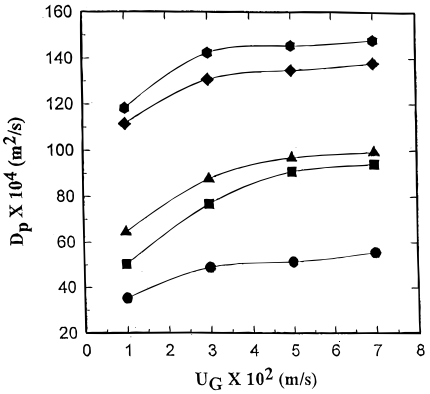

Figure 7. Effects of the gas flow rate on the mixing coefficients of particles of three different sizes. d_p (mm): (●) 1, (■) 3, (▲) 3, (◆) 6, (⬢) 6. U_L (m/s): (●) 0.10, (■) 0.08, (▲) 0.10, (◆) 0.12, (⬢) 0.14.

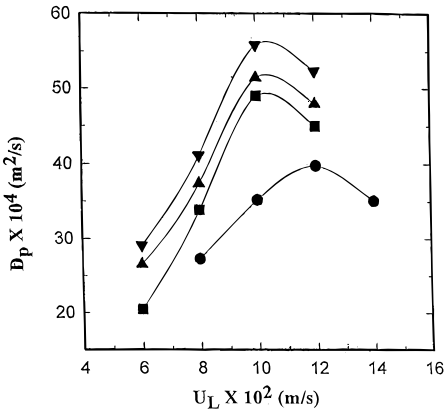

Figure 8. Effects of the liquid flow rate on the mixing coefficient of particles with a diameter of 1 mm (0.001 m). U_G (m/s): (●) 0.01, (■) 0.03, (▲) 0.05, (▼) 0.07.

of D_p on U_G is very similar to that of the gas holdup, ϵ_G, on U_G in gas−liquid−solid fluidized beds (Han et al., 1990).

Figures 8−10 present the effects of the liquid flow rate, U_L, on the particle-mixing coefficient, D_p, of particles of various individual sizes. These figures indicate that, in every bed, D_p increases with an increase in U_L when it is low, reaches a maximum, and then diminishes with a further increase in U_L. The range of U_L in which D_p attains its maximum is almost identical with that where the flow transition of fluidized

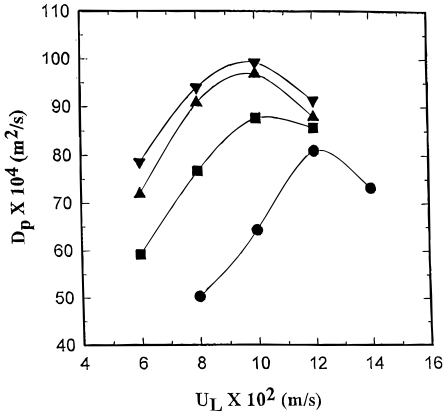

Figure 9. Effects of the liquid flow rate on the mixing coefficient of particles with a diameter of 3 mm (0.003 m). U_G (m/s): (●) 0.01, (■) 0.03, (▲) 0.05, (▼) 0.07.

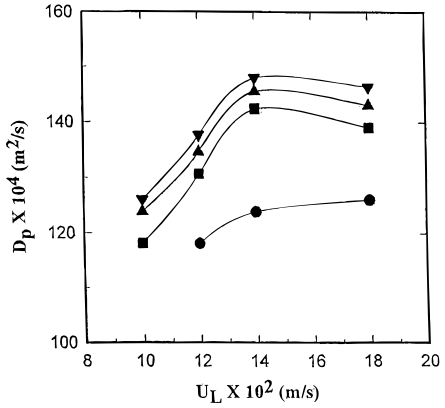

Figure 10. Effects of the liquid flow rate on the mixing coefficient of particles with a diameter of 6 mm (0.006 m). U_G (m/s): (●) 0.01, (■) 0.03, (▲) 0.05, (▼) 0.07.

particles would occur in gas−liquid−solid fluidized beds (Kang and Kim, 1988). This propensity has also been pointed out by Kang et al. (1997). According to Fan et al. (1987), D_p of particles of a given size, 3.0 mm (0.003 m) or 4.0 mm (0.004 m) in diameter, diminishes with increasing U_L at the relatively higher range of U_L; however, the values of D_p are not reported in the relatively lower range of U_L [less than 9 cm/s (0.09 m/s)], where D_p would increase with increasing U_L. It is highly plausible that in the intermediate range of U_L clearly discernible in Figure 8, the fluidizing liquid supplies sufficient energy to prevent clustering of the particles so that they can move individually; thus, it magnifies the particle-mixing coefficient, D_p.

Figure 11 shows the effects of the particle diameter, d_p, on the particle-mixing coefficient, D_p, of particles. D_p increases appreciably with an increase in d_p in the relatively higher range of the liquid flow rate, U_L. The larger d_p, the greater the minimum fluidization velocity, U_{mf}, and the range of U_L required for fluidization. Hence, a comparison of D_p's of the particles has been available only in the relatively higher range of U_L, specifically in the range exceeding 10 cm/s (0.1 m/s). This is particularly the case when the gas flow rate, U_G, is high and d_p is large. Both the gas holdup, ϵ_G, and the particle holdup, ϵ_S, are magnified with the increase in d_p (Han et al., 1990).

Fractal Characteristics of Pressure Fluctuations. To elucidate the effects of the gas flow rate, U_G, and the liquid flow rate, U_L, on the particle-mixing coefficient, D_p, in gas−liquid−solid fluidized beds, each

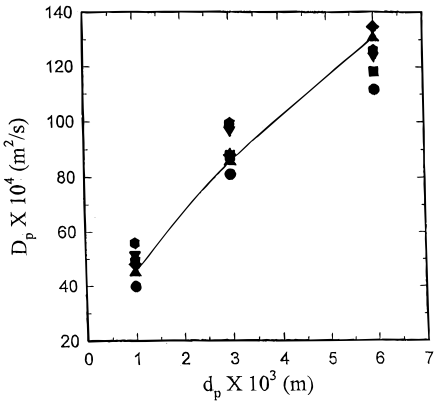

Figure 11. Effects of the particle size on the mixing coefficients under various flow conditions. U_G (m/s): (●) 0.01, (■) 0.03, (▲) 0.03, (▼) 0.05, (◆) 0.05, (⬢) 0.07. U_L (m/s): (●) 0.12, (■) 0.10, (▲) 0.12, (▼) 0.10, (◆) 0.12, (⬢) 0.10.

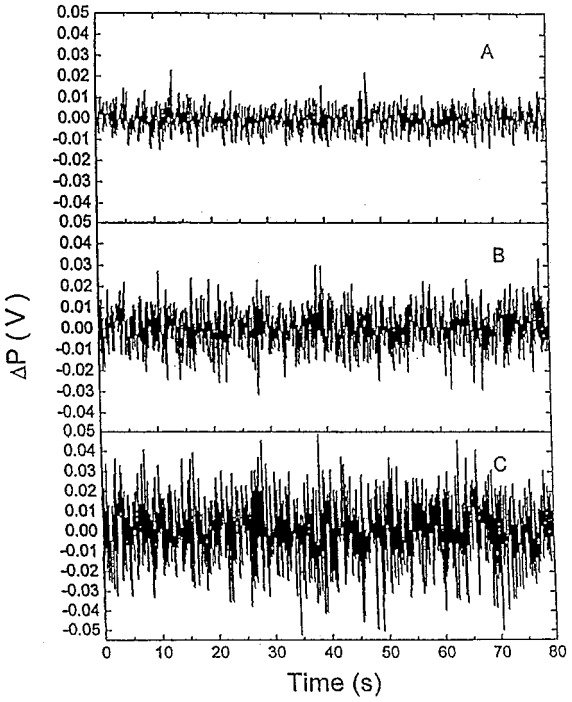

Figure 12. Typical pressure-fluctuation signals at three gas velocities (d_p = 1 + 3 mm, U_L = 0.10 m/s). U_G (m/s): (A) 0.01, (B) 0.03, (C) 0.05.

containing a binary-particle mixture, the pressure fluctuations were measured and the resultant data analyzed fractally (Fan et al., 1990, 1991, 1993; Kwon et al., 1994; Luewisuthichat et al., 1995; Kang et al., 1996). Figure 12 exhibits typical temporal records of pressure fluctuations in the bed of a binary-particle mixture (d_p = 1 mm + 3 mm or 0.001 m + 0.003 m), with each record plotted as a function of U_G. Note that the higher the U_G, the greater the amplitude and frequency of pressure fluctuations. The inference is that the mixing is intensified with the increase in U_G.

The rescaled range (R/S) resulting from the fractal analysis of pressure fluctuations correlates almost linearly with the time lag, τ, as can be seen in Figure 13. An individual value of the Hurst exponent, H, is recovered from the slope of this linear correlation with a correlation coefficient greater than 0.95 for all the data recorded. Illustrated in Figure 14 are the effects of the

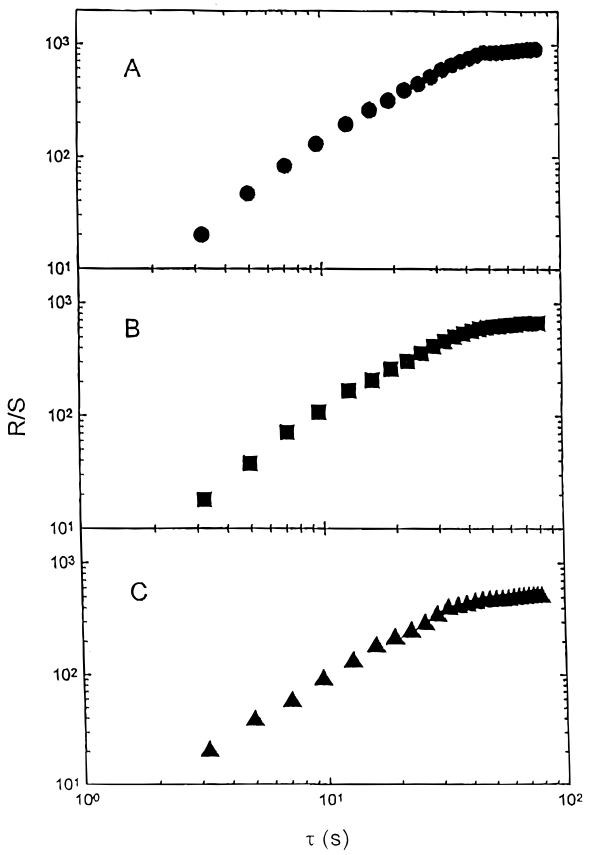

Figure 13. Pox diagram for pressure-fluctuation signals (d_p = 1 + 3 mm, U_L = 0.10 m/s). U_G (m/s): (A) 0.01, (B) 0.03, (C) 0.05.

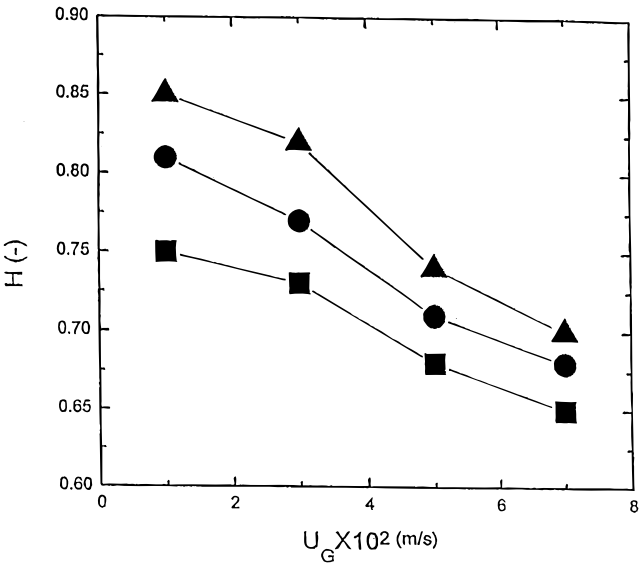

Figure 14. Effects of the gas flow rate on the Hurst exponent. d_p (mm): (■) 1 + 3, (●) 3 + 6, (▲) 3 + 6. U_L (m/s): (■) 0.10, (●) 0.10, (▲) 0.12.

gas flow rate, U_G, on H for the beds, each containing a binary-particle mixture. It can be seen that H decreases with increasing U_G, thus implying that the pressure fluctuations become less persistent. This, in turn, implies that the predictability of the beds' behavior diminishes with an increase in the gas holdup and the intensification of turbulence in the beds. In other words, the increase in U_G enhances the mixing and contacting among the various phases and between the particles of different sizes.

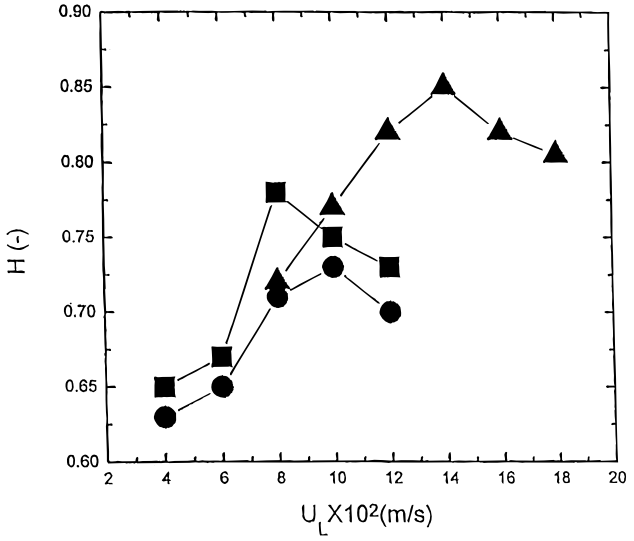

Figure 15. Effects of the liquid flow rate on the Hurst exponent. d_p (mm): (■) 1 + 3, (●) 3 + 6, (▲) 3 + 6. U_G (m/s): (■) 0.01, (●) 0.03, (▲) 0.03.

Figure 15 presents the variation of the Hurst exponent, H, with the liquid flow rate, U_L, in the beds of binary-particle mixtures; H exhibits a local maximum in each of the beds. It is worth noting that the range of U_L where H peaks approximately coincides with that where the particle-mixing coefficient, D_p, peaks, thereby indicating that the flow pattern and the mixing behavior of various phases in the beds are most persistent in the intermediate range of U_L. This may be due to the enhancement of periodic motion of particles in this range of U_L. In the lower range of U_L, the particles tend to flow in groups or clusters because each individual particle does not possess sufficient energy to travel freely and periodically. Nevertheless, in the higher range of U_L, sufficient energy provided to the particles and sufficient void created by bed expansion render it possible for the particles to travel freely without clustering.

Correlations. The particle-mixing coefficient, D_p, has been empirically correlated in terms of the operating variables as follows:

$$D_p = 45.36 U_G^{0.1482} U_L^{0.4622} d_p^{0.5875} \qquad (18)$$

The resultant correlation coefficient is 0.9473.

Particle mixing in gas−liquid−solid fluidized beds is profoundly influenced by the intensity of turbulence of the continuous liquid phase and energy dissipation in the beds; hence, D_p has also been correlated in terms of these two parameters. Based on Kolmogoroff's local isotropic turbulence theory, the Peclet number containing D_p has been correlated with the dimensionless particle diameter, d_p/D_T, which is regarded as the length scale of micro-eddies, and the dimensionless fluid flow rate, $U_L/(U_L + U_G)$, as shown.

$$Pe_p = \frac{U_L d_p}{D_p} = 1.48\left(\frac{d_p}{D_T}\right)\left(\frac{U_L}{U_L + U_G}\right)^{0.50} \qquad (19)$$

This expression fits well with the experimental data: the correlation coefficient is 0.9260; see Figure 16.

Concluding Remarks

Studies have been carried out on the axial-mixing characteristics and flow behavior of fluidized particles

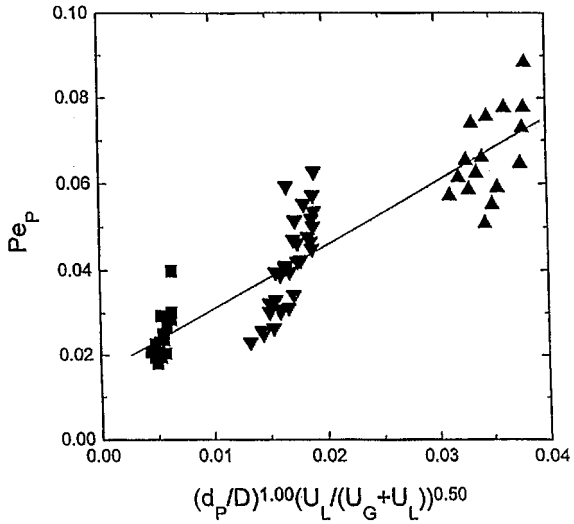

Figure 16. Correlation of the mixing coefficients of fluidized particles. d_p (mm): (■) 1, (▼) 3, (▲) 6.

of a binary mixture in a gas−liquid−solid bed. Specifically, the particle-mixing coefficients, D_p's, have been evaluated from the composition profiles of the particles in the bed. It has been found that D_p increases with an increase in the gas flow rate, U_G, or the particle size, d_p, and that it exhibits a local maximum with respect to the variation of the liquid flow rate, U_L. Such complex mixing behavior has been interpreted by means of the fractal analysis of pressure fluctuations in the bed. The analysis has yielded the Hurst exponent, H, which decreases with increasing U_G but displays a local maximum with the variation of U_L. D_p has been correlated in terms of the operating variables; moreover, the Peclet number containing D_p has been correlated with the dimensionless groups derived from the isotropic turbulence theory.

Nomenclature

A: cross-sectional area of a fluidized bed [m^2]
a, b: constant
$B(t,u)$: cumulative departure of $X(t+u)$ from the average for the subrecord between time $t + 1$ and time $t + \tau$
C: fractional volumetric concentration of particles
D: diameter of the column [m]
D_p: axial dispersion coefficient of the particles, i.e., particle-mixing coefficient [m^2/s]
d_p: particle diameter [m]
f: fraction in the fluid
g: gravitational acceleration [m/s^2]
H: Hurst exponent
L: bed height [m]
N: total particle flux [m/s]
ΔP: pressure difference in the bed [Pa]
Pe_p: Peclet number
$R(t,\tau)$: sample sequential rescaled range
$S^2(t,\tau)$: sample sequential variance
$\bar{U}_p$: bulk or convective velocity of a particle in the axial direction [m/s]
U: superficial velocity of fluid [m/s]
U_{f0}: effective volumetric flux of fluid in the bed of one component [m/s]
U_f: effective volumetric flux of fluid [m/s]
W: total mass of the particles [kg]
$X(t)$: pressure-fluctuation time series [v]
Z: axial height in the bed

Greek Letters

ϵ: holdup
ρ: density [kg/m^3]
τ: time lag [s]

Subscripts

f: fluid
i: sampling layer
G: gas
L: liquid
SL: large particles
SS: small particles
Z: axial direction

Literature Cited

Al-Dibouni, M. R.; Garside, J. Particle Mixing and Classification in Liquid Fluidized Bed. *Trans. Inst. Chem. Eng.* **1979**, *57*, 94−103.

Evstroperva, I. P.; Taganov, I. N.; Romankov, P. G. Experimental Study for the Rates of Motion of the Solid Phases in a Solid−Liquid−Gas System. *Theor. Found. Chem. Eng.* **1972**, *6*, 545−549.

Fan, L. S. *Gas−Liquid−Solid Fluidization Engineering*; Butterworth: Boston, 1989; pp 451−513.

Fan, L. S.; Chern, S. H.; Muroyama, K. Qualitative Analysis of Solids Mixing in a Gas−Liquid−Solid Fluidized Bed Containing a Binary Mixture of Particles. *AIChE J.* **1984**, *30*, 858−860.

Fan, L. S.; Matsuura, A.; Chern, S. H. Hydrodynamic Characteristics of a Gas−Liquid−Solid Fluidized Bed Containing a Binary Mixture of Particles. *AIChE J.* **1985**, *31*, 1801−1810.

Fan, L. S.; Yamashita, T.; Jeau, R. H. Solid Mixing and Segregation in a Gas−Liquid−Solid Fluidized Bed. *Chem. Eng. Sci.* **1987**, *42*, 17−25.

Fan, L. T.; Neogi, D.; Yashima, M.; Nassar, R. Stochastic Analysis of a Three-Phase Fluidized Bed: Fractal Approach. *AIChE J.* **1990**, *36*, 1529−1535.

Fan, L. T.; Neogi, D.; Yashima, M. *Elementary Introduction to Spatial and Temporal Fractal*; Springer: Heidelberg, Germany, 1991; pp 60−69.

Fan, L. T.; Kang, Y.; Neogi, D.; Yashima, M. Fractal Analysis of Fluidized Particle Behavior in Liquid−Solid Fluidized Bed. *AIChE J.* **1993**, *39*, 513−517.

Feder, J. *Fractals*; Plenum: New York, 1998, pp 149−183.

Han, J. H.; Will, G.; Kim, S. D. Phase Holdup Characteristics in Three Phase Fluidized Beds. *Chem. Eng. J.* **1990**, *23*, 67−73.

Juma, A. K. A.; Richardson, J. F. Segregation and Mixing in Liquid Fluidized Beds. *Chem. Eng. Sci.* **1983**, *38*, 955−967.

Kang, Y.; Kim, S. D. Solid Flow Transition in Liquid and Three Phase Fluidized Beds. *Part. Sci. Technol.* **1988**, *6*, 133−144.

Kang, Y.; Kim, S. D. Stochastic Analysis and Modeling of Three Phase Fluidized Beds. *Chem. Ind. Technol.* **1995**, *13*, 27−34.

Kang, Y.; Woo, K. J.; Ko, M. H.; Kim, S. D. Unsteady-State Behavior and Fluctuations of Fluidized Particles in Three Phase Fluidized Beds. *Hwahak Konghak* **1995**, *33*, 633−639.

Kang, Y.; Ko, M. H.; Kim, S. D.; Yashima, M.; Fan, L. T. Pressure Fluctuations and Particle Dispersion in Liquid Fluidized Beds. *AIChE J.* **1996**, *42*, 1164−1169.

Kang, Y.; Yashima, M.; Fan, L. T. Analysis of Random Behavior of Multiphase Flow in a Gas−Liquid−Solid Fluidized Bed. *First International Particle Technology Forum*, Denver, CO, Aug 17−19, 1994; pp 469−474.

Kang, Y.; Woo, K. J.; Ko, M. H.; Kim, S. D. Particle Dispersion and Pressure Fluctuations in Three-Phase Fluidized Beds. *Chem. Eng. Sci.* **1997**, in press.

Kim, S. D.; Kang, Y. Dispersed Phase Characteristics in Three-Phase Fluidized Bed, Mixed-flow Hydrodynamics. *Advances in Engineering Fluid Mechanics*; Cheremisinoff, N. P., Ed.; Gulf Pub. Co.: Houston, TX, 1996; pp 845−869.

Kwon, H. W.; Kang, Y.; Kim, S. D.; Yashima, M.; Fan, L. T. Bubble Chord Length and Pressure Fluctuations in Three-Phase Fluidized Beds. *Ind. Eng. Chem. Res.* **1994**, *33*, 1852−1857.

Larachi, F.; Cassanello, M.; Marie, M.; Chaouki, J.; Guy, C. Solid Circulation Patterns in Three-Phase Fluidized Beds Containing Binary Mixtures of Particles as Inferred from RPT. *Trans. Inst. Chem. Eng.* **1995**, *73*, 263−268.

Luewisuthichat, W.; Tsutsumi, A.; Yoshida, K. Fractal Analysis of Particle Trajectories in Three-Phase Systems. *Trans. Inst. Chem. Eng.* **1995**, *73*, 222−227.

Yutani, H.; Ototake, H.; Too, J. R.; Fan, L. T. Estimate of the Particle Diffusivity in a Liquid−Solids Fluidized Bed Based on a Stochastic Model. *Chem. Eng. Sci.* **1992**, *37*, 1079−1085.

Received for review December 8, 1997
Revised manuscript received July 13, 1998
Accepted July 23, 1998

IE9708900